Registration of anatomical images using geodesic paths of diffeomorphisms parameterized with stationary vector fields

Monica Hernandez, Matias N. Bossa, and Salvador Olmos
Communication Technologies Group (GTC) and
Aragon Institute of Engineering Research (I3A)
University of Zaragoza, Spain
{mhg,bossa,olmos}@unizar.es

Abstract

Computational Anatomy aims for the study of the statistical variability in anatomical structures. Variability is encoded by the transformations existing among populations of anatomical images. These transformations are usually computed from diffeomorphic registration based on the large deformation paradigm. In this framework diffeomorphisms are usually computed as end points of paths on the Riemannian manifold of diffeomorphisms parameterized by non-stationary vector fields. Recently, an alternative parameterization based on stationary vector fields has been developed. In this article we propose to use this stationary parameterization for diffeomorphic registration. We formulate the variational problem related to this registration scenario and derive the associated Euler-Lagrange equations. We evaluate the performance of the non-stationary vs the stationary parameterizations in real and synthetic 3D-MRI datasets. Compared to the non-stationary parameterization, our proposal provides similar accuracy in terms of image matching and deformation smoothness while drastically reducing memory and time requirements.

1. Introduction

Computational Anatomy aims for the study of the statistical variability in anatomical structures. Variability is encoded by the transformations existing among anatomical images. The statistical analysis of these transformations allows modeling the anatomical variability of a population. From this analysis, statistical inference can be used in order to identify anatomical differences between healthy and diseased individuals or improve the diagnosis of pathologies [11, 15, 20]. In this framework, transformations are usually assumed to belong to a group of diffeomorphisms (i.e. differentiable maps with differentiable inverse) endowed with the structure of Riemannian manifold.

In Computational Anatomy, diffeomorphic registration has been approached in the large deformation setting as a variational problem that combines the minimization of an image matching energy functional with a regularizing constraint on the diffeomorphic transformation. The image matching functional has been usually selected as the sum of squared intensity differences or information theory measures [6, 4, 14]. Transformations have been represented as end points of paths of diffeomorphisms parameterized by time-varying smooth vector fields defined on the tangent space. In the last years, some variations in the definition of the elements of the variational problem have been proposed providing different algorithms for diffeomorphic registration. Joshi et al. have proposed an inverse consistent version of the variational problem that incorporates a source to target symmetry in the registration [13]. Avants et al. have combined landmark based diffeomorphic registration in this inverse consistent framework [3]. L. Younes has proposed to restrict the optimization to paths that fulfill the momentum conservation [21]. This constraint guarantees that the solutions to the diffeomorphic registration problem lie on the geodesics of the manifold. This is very desirable for further Riemannian statistical analysis [8, 17]. Garcin et al. have defined a Riemannian manifold structure on the space of anatomical images in order to find geodesic paths on the manifold of diffeomorphisms as well as on the image manifold [9].

Recently, an alternative way of parameterizing paths of diffeomorphisms has been proposed in [2]. The parameterization is obtained using stationary smooth vector fields defined on the tangent space. This parameterization is closely related to the group structure defined on the Riemannian manifold of diffeomorphisms as the paths that can be parameterized using stationary vector fields are exactly

[0]This work has been partially supported by research grants TEC2006-13966-C03-02 and FIS PI04/1795. M.N. Bossa work is funded by DGA under the FPI grant B097/2004.

978-1-4244-1631-8/07/$25.00 ©2007 IEEE

geodesic paths identified with one-parameter subgroups. To our knowledge, the stationary parameterization has not been used for diffeomorphic registration.

In this article, we propose to use the stationary parameterization for diffeomorphic registration in the variational problem studied in Computational Anatomy. This restricts transformations to belong to geodesic paths identified with some one-parameter subgroup on the manifold. We formulate the variational problem related to the registration scenario and derive the Euler-Lagrange equations associated to the minimization of the energy functional. We evaluate the performance of the non-stationary vs the stationary parameterizations in real and synthetic 3D-MRI datasets.

The rest of the article is divided as follows. In Section 2 we revisit the differential structure of the Riemannian manifold of diffeomorphisms. In Section 3 we present our method for diffeomorphic registration. Results in real and synthetic datasets are presented in Section 4. Finally, Section 5 presents discussion and some concluding remarks.

2. Riemannian manifolds of diffeomorphisms

In this section we describe the differentiable structure of the Riemannian manifold

$$Diff(\Omega) := \{\varphi : \Omega \to \Omega, \varphi \text{ and } \varphi^{-1} \text{ smooth mappings}\} \tag{1}$$

as well as the two different parameterizations of paths of diffeomorphisms that have been proposed in the literature. The set Ω is a compact simply connected manifold. In our framework, Ω represents the image domain that is a compact cubic neighborhood of points in $\mathbb{R}^3$.

The study of infinite dimensional manifolds is more complicated than in finite dimensions. In the finite dimensional case the structure of differentiable manifold provides a local homeomorphism from every element in the manifold to the Euclidean vector space, $\mathbb{R}^n$. Thus, finite dimensional manifolds locally behave like Euclidean spaces. Otherwise, infinite dimensional differentiable manifolds are locally homeomorphic to infinite dimensional metric vector spaces (namely, a Frechet, a Banach or a Hilbert space), showing a complex differential structure. In every point of the manifold, this vector space is the so called tangent space (V). In the case of $Diff(\Omega)$, this is the vector space of smooth vector fields in Ω. Depending on the degree of differentiability of the set of diffeomorphisms (i.e. the meaning of the term "smooth" in Equation 1), we can obtain different metric spaces and, therefore, different structures of differentiable manifold in $Diff(\Omega)$. For example, the set of C^∞ diffeomorphisms $Diff^\infty(\Omega)$ is a Frechet space, the set of C^k, $k < \infty$, diffeomorphisms $Diff^k(\Omega)$ is a Banach space, and the set of Sobolev H^s, $s > \frac{1}{2}\dim(\Omega)$ diffeomorphisms $Diff^s(\Omega)$ is a Hilbert space [18].

In Computational Anatomy, Riemannian manifolds of diffeomorphisms are considered with the Hilbert differentiable structure. $Diff^s(\Omega)$ has been widely studied in physics [1, 12, 7] as the computation of the motion of a system in continuum mechanics can be described by a path of diffeomorphisms

$$\phi : [0,1] \to Diff^s(\Omega), t \to \phi(t) \tag{2}$$

deforming the ambient space Ω. The analogies existing between this physical problem and diffeomorphic registration allow to translate the setting for working with $Diff^s(\Omega)$ from continuum mechanics to Computational Anatomy.

Thus, in both disciplines paths of diffeomorphisms are usually parameterized as the solution of the transport equation

$$\dot{\phi}(t) = v(t, \phi(t)) \tag{3}$$

with initial condition $\phi(0) = id$, where $v : [0,1] \to V$ is a time varying flow of smooth vector fields in the tangent space V. Diffeomorphisms can be computed as solutions of non-stationary ordinary differential equations (ODE). The metric in $Diff^s(\Omega)$ is defined from the scalar product $\langle v, w \rangle_V = \langle Lv, Lw \rangle_{L^2}$ where L is a linear invertible differential operator. The Hilbert differentiable structure guarantees that the solution to the transport equation is a path of diffeomorphisms in $Diff^s(\Omega)$. [1]

With this parameterization, the energy of a path in the Riemannian manifold is defined as

$$E(\phi) = \sqrt{\int_0^1 \|v(t)\|_V^2 dt} \tag{4}$$

This energy intuitively represents the cost that supposes walking on the manifold following that path. Paths minimizing this cost are called geodesic curves. In this case, the energy is identified with the metric and measures the amount of deformation associated to the diffeomorphism $\phi(1)$.

Recently, an alternative way of parameterization of geodesics in $Diff^s(\Omega)$ has been proposed [2]. In this framework, geodesic paths are parameterized as the solution of the transport equation associated to a stationary smooth vector field in the tangent space,

$$\dot{\phi}(t) = w(\phi(t)) \tag{5}$$

with initial condition $\phi(0) = id$, where $w \in V$. With this parameterization diffeomorphisms can be computed as solutions of stationary ODEs. The energy of a path parameterized by a stationary vector field w can be defined from Equation 4 as

$$E(\phi) = \sqrt{\int_0^1 \|tw\|_V^2 dt} = \|w\|_V \tag{6}$$

[1] In fact, the solution does not exist in $Diff^\infty(\Omega)$ and $Diff^k(\Omega)$ as these spaces are not Sobolev.

This parameterization is closely related to the group structure defined in $Diff^s(\Omega)$ with the right invariant metric defined in Equation 4 as the geodesic paths that can be parameterized using stationary vector fields are exactly the one-parameter subgroups. In this case, the vector field w is an infinitesimal generator of the subgroup and the solution of the transport equation is identified with the exponential map. It has been shown that this set of diffeomorphisms do not comprise all diffeomorphisms in $Diff^s(\Omega)$ (in fact, the exponential map is not onto [10]). Nevertheless, it could provide good results for diffeomorphic registration of anatomical images as well as an appropriate framework for further Riemannian statistical analysis [8, 17].

3. Diffeomorphic registration of anatomical images

In this article, diffeomorphic registration from a template image I_0 to a target I_1 is obtained computing the end point φ of a path of diffeomorphisms $\phi(t)$ resulting from the minimization of the energy functional

$$E(\varphi) = E(\phi)^2 + \frac{1}{\sigma^2}\|I_0 \circ \varphi^{-1} - I_1\|^2_{L^2} \qquad (7)$$

where $E(\phi)$ measures the energy of the path $\phi(t)$, $\|\cdot\|_{L^2}$ measures the matching between the images after registration and the scaling factor σ balances the energy contribution between deformation and image differences. In this section we review the method for diffeomorphic registration using the non stationary parameterization and formulate our method using the stationary parameterization.

3.1. Registration using the non-stationary parameterization

In Computational Anatomy, the energy functional 7 is usually written as

$$E_{I_0 \to I_1}(v(t)) = \int_0^1 \|v(t)\|^2_V dt + \frac{1}{\sigma^2}\|I_0 \circ \phi(1)^{-1} - I_1\|^2_{L^2} \qquad (8)$$

where $v(t)$ is the time-varying vector field parameterizing the path of diffeomorphisms $\phi(t)$ [4]. In order to assure a source to target symmetry in the registration, in this article we use the inverse-consistent version instead [13]

$$\begin{aligned} E_{I_0 \leftrightarrow I_1}(v(t)) \quad = \quad & \int_0^1 \|v(t)\|^2_V dt + \\ & \frac{1}{\sigma^2}\left(\|I_0 \circ \phi(1)^{-1} - I_1\|^2_{L^2}\right) + \\ & \frac{1}{\sigma^2}\left(\|I_1 \circ \phi(1) - I_0\|^2_{L^2}\right) \end{aligned} \qquad (9)$$

The Euler-Lagrange equation associated to the minimization of this energy functional is given in Equation 10. In this equation, L is a linear invertible differential operator associated to the $\|\cdot\|_V$. The time-varying vector field solution of the Euler-Lagrange equation provides a path of diffeomorphisms with minimal energy and maximum image matching at $t = 1$.

3.2. Registration using the stationary parameterization

In our method for diffeomorphic registration between anatomical images we parameterize diffeomorphisms as solutions of stationary ODEs belonging to a one-parameter subgroup for some infinitesimal generator $w \in V$. Thus, the diffeomorphism that connects I_0 and I_1 is represented by the exponential map $\exp(w)$, where w is computed from the minimization of the energy functional

$$\begin{aligned} E_{I_0 \leftrightarrow I_1}(w) = \|w\|^2_V \quad + \quad & \frac{1}{\sigma^2}\left(\|I_0 \circ \exp(w)^{-1} - I_1\|^2_{L^2}\right) + \\ & \frac{1}{\sigma^2}\left(\|I_1 \circ \exp(w) - I_0\|^2_{L^2}\right) \end{aligned} \qquad (11)$$

The Euler-Lagrange equation associated to the minimization of the energy functional is given in Equation 12. The details of the computation are given in the Appendix. The stationary vector field solution of the Euler-Lagrange equation provides a one-parameter subgroup of diffeomorphisms with minimal deformation and maximum image matching at $t = 1$.

3.3. Numerical implementation

The numerical implementation for finding the minimum of the energy functionals $E_{I_0 \leftrightarrow I_1}(v(t)))$ and $E_{I_0 \leftrightarrow I_1}(w)$ proceeds within a multi-resolution strategy in a gradient descent fashion. In order to make both algorithms comparable, the same implementational criteria have been adopted in their common stages.

In the coarsest resolution level, the algorithm based on the non-stationary parameterization initializes with iteration $k = 0$, $v(t) = 0_V$ and $\phi(t) = id\ \forall t$ whereas the algorithm based on the stationary parameterization initializes with $w = 0_V$, and $\varphi = id$. In the finer resolution levels, both algorithms initialize $v(t)$ and w interpolating the vector fields resulting from the convergence in the previous resolution level using a b-spline interpolator. Every iteration in the gradient descent consists of the steps collected in Table 1.

In both algorithms, a golden search strategy based on the optimization scheme in [4] is used to update the step size ϵ. The computation of the diffeomorphisms is performed by solving the transport equations 3 and 5 using a semi-lagrangian algorithm [19]. The operator associated to $\langle ., . \rangle_V$

$$\nabla_{v(t)} E(v(t)) = 2v(t) - \frac{2}{\sigma^2}(LL^\dagger)^{-1}\left(\det(D\phi(t)^{-1})(I_0 \circ \phi(t)^{-1} - I_1 \circ \phi(T-t))(\nabla I_0(\phi(t)^{-1}) + \nabla I_1(\phi(T-t)))\right) \tag{10}$$

$$\nabla_w E(w) = 2w - \frac{2}{\sigma^2}(LL^\dagger)^{-1}\left((I_0 \circ \exp(w)^{-1} - I_1)\nabla(I_0 \circ \exp(w)^{-1}) + (I_1 \circ \exp(w) - I_0)\nabla(I_1 \circ \exp(w))\right) \tag{12}$$

is selected to be $L = \gamma Id - \alpha\nabla^2$, and $LL^\dagger$ is computed in the Fourier domain as in [4]. The convergence in each resolution level is reached if the value of ϵ in the search strategy is too small or the rate of change in the energy is less than a tolerance value.

4. Results

In this section we provide the evaluation of our method for diffeomorphic registration. This evaluation consists in comparing the performance of the non-stationary and the stationary parameterizations in the registration scenarios associated to the variational problems $E_{I_0 \leftrightarrow I_1}(v(t))$ and $E_{I_0 \leftrightarrow I_1}(w)$. We provide results on real and synthetic MRI brain datasets.

4.1. Real datasets

The population of real anatomical brain images was composed by a total of 18 T1-MRI from the Hospital Clinic Barcelona, Spain. The images were acquired using a General Electric Signa Horizon CV 1.5 Tesla scan. As preprocessing steps, the images were first re-sampled yielding volumes of size $256 \times 256 \times 220$ with a spatial resolution of $0.9 \times 0.9 \times 0.9$ mm and cropped to volumes of size $155 \times 205 \times 170$. Next, the skull was removed from the images [5]. Finally, the image intensity was normalized using a histogram matching algorithm and all the images were aligned to a common coordinate system using a similarity transformation (7 dof) with the algorithms available at the Insight Toolkit (ITK).

4.2. Registration in real datasets

In this experiment, we evaluate the performance of the diffeomorphic registration algorithms in real datasets. The quality of the registration is measured with parameters based not only on the final image matching but also on the transformation smoothness. The image matching is quantified from the relative L^2 differences,

$$RSSD = \frac{1}{2}\frac{\|I_0 \circ \varphi^{-1} - I_1\|_{L^2} + \|I_1 \circ \varphi - I_0\|_{L^2}}{\|I_0 - I_1\|_{L^2}} \tag{13}$$

This measure comprises errors in the registration due to photometric variations between the images and inaccurate matching consequence of diffeomorphic regularization constraints. The smoothness of the transformation is measured from the extrema of the Jacobian determinant associated to the inverse transformation, $J_{max} = \max(\det(D\varphi^{-1}))$ and $J_{min} = \min(\det(D\varphi^{-1}))$. From those registrations with the same relative differences the ones with the highest minimum determinant (i.e. smoother) are more desirable.

As these performance parameters are strongly influenced by the selection of the scaling parameter σ, the experiment consists in the registration of one of the images randomly selected in our datasets to the rest of images with several values of σ. Table 2 presents the average and standard deviation of these measurements obtained in the experiment. Figure 1 shows a representative example of diffeomorphic registration with this parameter setting. The histogram of the differences between the template, the target and the corresponding transformed images is shown in Figure 2.

Table 2. Registration in real datasets. Average and standard deviation of the relative L^2 differences, $RSSD$, and the extrema of the jacobian determinant, J_{max}, J_{min}. Upper and lower tables show the results obtained with $E_{I_0 \leftrightarrow I_1}(w)$ and $E_{I_0 \leftrightarrow I_1}(v(t))$, respectively.

	$1/\sigma^2$	$RSSD$	J_{min}	J_{max}
$E_{I_0 \leftrightarrow I_1}(w)$	1e0	0.66 ± 0.04	0.82 ± 0.02	1.21 ± 0.03
	5e1	0.36 ± 0.04	0.36 ± 0.14	2.25 ± 0.57
	1e2	0.32 ± 0.03	0.29 ± 0.14	3.10 ± 1.31
	5e2	0.30 ± 0.03	0.26 ± 0.14	3.79 ± 2.31
	1e3	0.27 ± 0.02	0.23 ± 0.14	4.37 ± 2.75
	5e3	0.27 ± 0.02	0.23 ± 0.13	4.15 ± 2.31
	1e4	0.26 ± 0.02	0.23 ± 0.13	4.13 ± 2.34
	5e4	0.26 ± 0.01	0.23 ± 0.13	4.23 ± 2.53
	1e5	0.27 ± 0.02	0.23 ± 0.13	4.10 ± 2.18
	$1/\sigma^2$	$RSSD$	J_{min}	J_{max}
$E_{I_0 \leftrightarrow I_1}(v(t))$	1e0	0.66 ± 0.04	0.68 ± 0.01	1.39 ± 0.03
	5e1	0.37 ± 0.04	0.30 ± 0.20	2.19 ± 0.56
	1e2	0.34 ± 0.04	0.29 ± 0.12	2.89 ± 1.26
	5e2	0.31 ± 0.03	0.25 ± 0.11	3.76 ± 2.32
	1e3	0.29 ± 0.02	0.22 ± 0.12	4.17 ± 2.74
	5e3	0.28 ± 0.02	0.21 ± 0.08	4.29 ± 2.62
	1e4	0.27 ± 0.02	0.19 ± 0.10	4.35 ± 2.58
	5e4	0.27 ± 0.02	0.19 ± 0.11	4.27 ± 2.30
	1e5	0.27 ± 0.02	0.19 ± 0.09	4.56 ± 2.55

Table 1. Algorithms for diffeomorphic registration. Left, registration using the non-stationary parameterization. Right, registration using the stationary parameterization.

(1) Compute $\nabla_{v_k(t)} E(v_k(t))$ from the Euler-Lagrange Equation 10.
(2) Update the gradient descent step $v_k(t) = v_{k-1}(t) - \epsilon \nabla_{v_{k-1}(t)} E(v_{k-1}(t))$.
(3) Compute the inverse path of diffeomorphimsms $\phi^{-1}(t)$.
(4) Compute the direct path of diffeomorphisms $\phi(t)$.
(5) Compute the transformed images $I_0 \circ \phi^{-1}(t)$ and $I_1 \circ \phi(t)$.
(6) Check for convergence criterion.
(7) Prepare the next resolution level.

(1) Compute $\nabla_{w_k} E(w_k)$ from the Euler-Lagrange Equation 12.
(2) Update the gradient descent step $w_k = w_{k-1} - \epsilon \nabla_{w_{k-1}} E(w_{k-1})$.
(3) Compute the inverse diffeomorphimsm $\varphi^{-1} = \exp(-w_k)$.
(4) Compute the direct diffeomorphism $\varphi = \exp(w_k)$.
(5) Compute the transformed images $I_0 \circ \varphi^{-1}$ and $I_1 \circ \varphi$.
(6) Check for convergence criterion.
(7) Prepare the next resolution level.

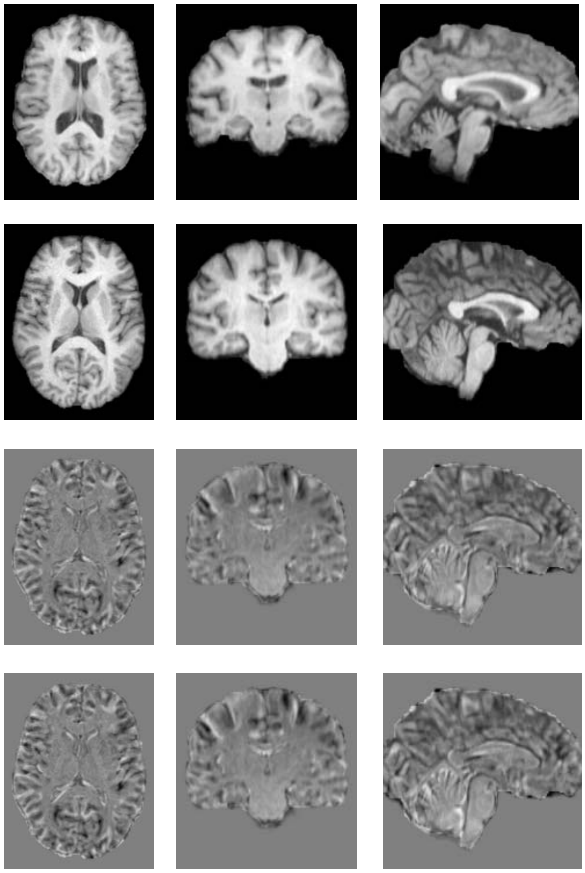

Figure 1. Illustration of axial, coronal and saggital views of a real data registration experiment for $1/\sigma^2 = 5.0e4$. The first and second rows show the template (I_0) and the target (I_1) used for registration. The third and fourth rows show the differences (ranging from -50 to 50) between the target and the deformed template obtained with $E_{I_0 \leftrightarrow I_1}(w)$ and $E_{I_0 \leftrightarrow I_1}(v(t))$, respectively. The image matching was equal to 0.26 in the case of stationary parameterization and 0.30 in the case of non-stationary parameterization. The corresponding jacobian values ranged from 0.23 to 12.30 and from 0.30 to 9.09, respectively.

4.3. Synthetic datasets

The population of synthetic anatomical brain images was composed by two groups of 20 images. Each group was generated from simulated diffeomorphic deformations parameterized with stationary and non-stationary vector fields applied to a template image randomly selected from the real datasets.

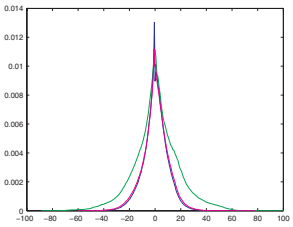

Figure 2. Histogram of the intensity differences in the registration experiment shown in Figure 1. Green plot corresponds to the differences before registration ($I_0 - I_1$). Blue and magenta plots correspond to the differences after registration using the stationary and the non-stationary parameterizations, respectively ($I_0 \circ \varphi^{-1} - I_1$ and $I_0 \circ \phi(1)^{-1} - I_1$). The histogram has been plotted just taking into account differences not equal to zero.

The stationary diffeomorphisms were simulated from the stationary vector fields $w_1, ..., w_N$ resulting from the registration of the template to the rest of the images in the real datasets. Principal Geodesic Analysis (PGA) was performed on the covariance matrix associated to the w_i using the method in [20]. New instances of stationary vector fields were generated from the modes of variation $u_1, ..., u_N$ and the corresponding eigenvalues $\lambda_1, ..., \lambda_N$ as $w_{\text{new}} = \Sigma_{i=1}^{N} \alpha_i \lambda_i u_i$. The parameters α_i were randomly selected from a normal distribution of zero mean and standard deviation 1. The simulated diffeomorphisms were obtained solving the stationary transport equation.

The simulated non-stationary diffeomorphisms were generated from the non-stationary vector fields $v_1(t), ..., v_N(t)$ resulting from the registration of the template to the rest of the images in the real datasets. As the space of time-varying vector fields is not linear, the computation of PGA was applied to the linear space of initial vector fields $v_1(0), ..., v_N(0)$ instead. This way, new instances of initial vector fields were generated as explained in the stationary case. The non-stationary vectors associated to the simulated initial vector fields were generated via geodesic shooting [16]. The simulated diffeomorphisms were obtained solving the non-stationary transport equation.

4.4. Registration in synthetic datasets

In this experiment, we evaluate the performance of the diffeomorphic registration algorithms in synthetic datasets. The quality of the registration is measured with parameters

based on the final image matching ($RSSD$). As photometric variations between the template and target images are null this measure comprises the errors in the registration due to inaccurate matching consequence of diffeomorphic regularization constraints (i.e. the parameterization used). In addition, we compare the simulated diffeomorphisms with the ones obtained via registration using the average L^2 differences (SSD) between corresponding grid points.

Table 3 presents the average and standard deviation of these measurements. Figures 3 and 4 show representative examples of the diffeomorphic registration experiments. The histogram of the differences before and after registration are shown in Figure 5.

Table 3. Registration in synthetic datasets. Average and standard deviation of the relative L^2 differences between the images, $RSSD$, and L^2 distance to the real transformations, SSD. Left table shows results corresponding to the simulated stationary diffeomorphic transformations and right table shows results corresponding to the non-stationary ones.

	$RSSD$	SSD	$RSSD$	SSD
$E_{I_0 \leftrightarrow I_1}(w)$	0.03 ± 0.00	0.48 ± 0.45	0.02 ± 0.01	0.44 ± 0.35
$E_{I_0 \leftrightarrow I_1}(v(t))$	0.03 ± 0.01	0.50 ± 0.46	0.03 ± 0.01	0.45 ± 0.37

4.5. Computational complexity

Computational complexity is measured in terms of memory and time requirements. The optimization for diffeomorphic registration in $E_{I_0 \leftrightarrow I_1}(v(t))$ and $E_{I_0 \leftrightarrow I_1}(w)$ requires the storage in memory of the diffeomorphic path parameterizations ($v(t)$ and w, respectively) and the corresponding energy gradients ($\nabla E_{v(t)}(t)$ and ∇E_w, respectively). If the path of diffeomorphisms in the non-stationary parameterization is sampled into T pieces, the memory requirements in this algorithm are multiplied by this parameter. Besides, the computation of the energy gradient requires the extra storage of the whole direct and inverse diffeomorphic paths in the case of non-stationary parameterization while the stationary parameterization requires the storage of just the direct and inverse diffeomorphisms. Thus, depending on the sampling T of the interval $[0, 1]$ in the non-stationary parameterization, the memory requirements of the non-stationary registration algorithm grow up to $k \cdot T$ times ours for some k. Time requirements are also multiplied by this factor. As example[2], in a volume of size $155 \times 205 \times 170$ registration using the non-stationary parameterization in the finer resolution level required up to 1.9 GB while stationary parameterization required about 800 MB. Time requirements for a single iteration took up to 143.20 seconds using the non-stationary parameterization whereas the stationary parameterization took 10.25 seconds in a machine of 2327 MHZ. This supposes a reduction of the whole registration algorithm from some hours to a few minutes.

[2]Code implemented in C++ based on the ITK library

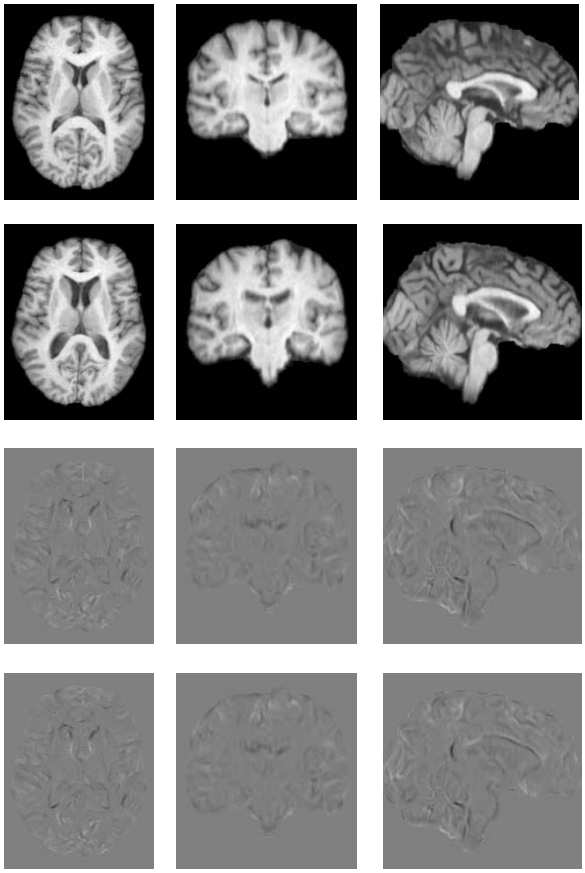

Figure 3. Illustration of axial, coronal and saggital views of a synthetic data registration experiment generated from a stationary diffeomorphism for $1/\sigma^2 = 5.0e4$. The first and second rows show the template (I_0) and the target (I_1) used for registration. The third and fourth rows show the differences (ranging from -50 to 50) between the target and the deformed template obtained with $E_{I_0 \leftrightarrow I_1}(w)$ and $E_{I_0 \leftrightarrow I_1}(v(t))$, respectively. The image matching was equal to 0.04 in the case of stationary parameterization and 0.04 in the case of non-stationary parameterization.

5. Discussion and conclusions

In this article, we have presented a method for diffeomorphic registration based on the large deformation paradigm studied in Computational Anatomy. In contrast to traditional methods, we estimate the optimal transformation connecting two anatomical images constrained to lie on geodesic paths parameterized by stationary vector fields.

The performance of the stationary vs non-stationary parameterizations has been compared in a set of 18 MRI real datasets. Both algorithms have similar accuracy and smoothness (in the optimal case shown in Table 2, the average $RSSD$ resulted to be 0.26 vs 0.27 and the average minimum Jacobian 0.23 vs 0.19). Besides, the differences before and after registration were reduced in the same degree in both cases (Figure 2). In the example shown in Figure 1, subcortical structures presented a maximum matching. However, the image matching seems to fail in the cortex. This may be due to the differences of intensity between

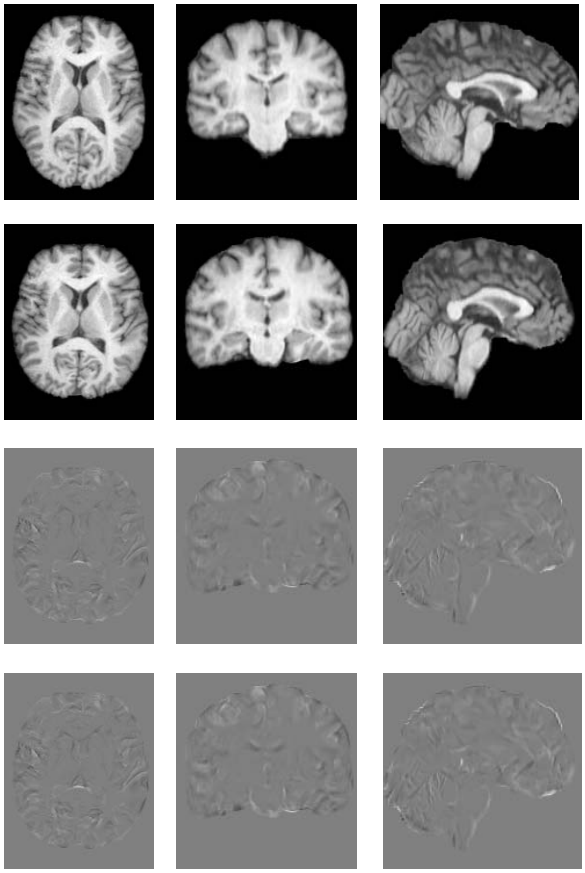

Figure 4. Illustration of axial, coronal and saggital views of a synthetic data registration experiment generated from a non-stationary diffeomorphism for $1/\sigma^2 = 5.0e4$. The first and second rows show the template (I_0) and the target (I_1) used for registration. The third and fourth rows show the differences (ranging from -50 to 50) between the target and the deformed template obtained with $E_{I_0 \leftrightarrow I_1}(w)$ and $E_{I_0 \leftrightarrow I_1}(v(t))$, respectively. The image matching was equal to 0.02 in the case of stationary parameterization and 0.02 in the case of non-stationary parameterization.

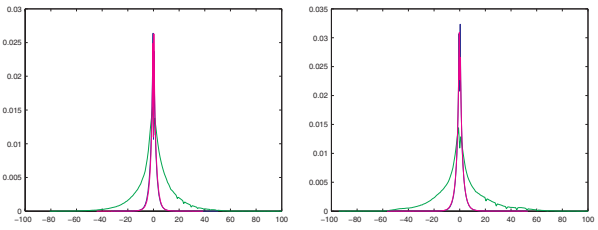

(a) (b)

Figure 5. Histogram of the intensity differences in the registration experiment shown in Figures 3 and 4, respectively. Green plot corresponds to the differences before registration. Blue and magenta plots correspond to the differences after registration using the stationary and the non-stationary parameterizations, respectively. The histogram has been plotted just taking into account differences not equal to zero.

images are higher in these regions of the brain. Another reason could be that the regularization constraints imposed on diffeomorphic registration makes the transformation not able to warp between structures with high geometrical variability.

In addition, the performance of both algorithms has been compared in two populations of 20 MRI datasets generated from simulated stationary and non-stationary parameterized diffeomorphisms. As pointed out by Table 3 and supported by Figures 3, 4, and 5, both algorithms have shown a high image matching (average $RSSD$ less than 0.03 in all cases) regardless the parameterization used to generate the diffeomorphism. The average differences of corresponding grid points between the simulated diffeomorphisms and the ones obtained via registration resulted to be within voxel resolution.

As a consecuence of the non surjectivity of the exponential map there exist points arbitrarilly close to the identity that cannot be parameterized by stationary vector fields. This means that there may exist two images where the non-stationary parameterization would provide much better registration performance than the stationary parameterization. However, the experiments reported in this article have shown that, at least for MRI brain images, one can find elements from both parameterizations that provide similar and acceptable registration results.

Regarding time and memory requirements, our algorithm has shown to provide a considerable reduction of the computational requirements for registration with identical accuracy results. For this reason, our algorithm may provide an alternative fast method for computing diffeomorphic registration in state of the art Computational Anatomy applications. Moreover, our algorithm allows to generate elements belonging to one-parameter subgroups of diffeomorphisms where the exponential and logarithm maps can be computed. Therefore it may be suitable to be used in a framework for Riemannian statistical analysis in the manifold of diffeomorphisms.

A. Euler-Lagrange equation for diffeomorphic registration

In this appendix, we present the computations to obtain the Euler-Lagrange equation for the energy functional given in Equation 11. In general convex vector spaces, the Euler-Lagrange equation associated to an energy functional $E(w)$ is obtained from $\nabla_w E(w) = 0$. In Frechet spaces, the gradient operator relates the Frechet derivative and the Gateaux derivative by $\partial_h E(w) = \langle \nabla_w E(w), h \rangle_V$. Thus, in our case, the Euler-Lagrange equation is computed from Gateaux derivatives. The Gateaux derivative of the energy functional along $h \in V$ is defined as the variation of $E(w)$ under the perturbation of w in the direction of h

$$\partial_h E(w) = \lim_{\epsilon \to 0} \frac{E(w + \epsilon h) - E(w)}{\epsilon} \tag{14}$$

For simplicity, we divide the computation of $\partial_h E(w)$ into $\partial_h E_1(w)$, $\partial_h E_2(w)$, and $\partial_h E_3(w)$ where

$$E_1(w) = \|w\|_V^2, \tag{15}$$

$$E_2(w) = \frac{1}{\sigma^2}\|I_0 \circ \exp(w)^{-1} - I_1\|_{L^2}^2, \text{ and} \tag{16}$$

$$E_3(w) = \frac{1}{\sigma^2}\|I_1 \circ \exp(w) - I_0\|_{L^2}^2. \tag{17}$$

Straightforward computations provide

$$\partial_h E_1(w) = 2\langle w, h\rangle_V \tag{18}$$

The chain rule allows to compute the variation of $E_2(w)$ and $E_3(w)$

$$\begin{aligned}\partial_h E_2(w) &= \frac{2}{\sigma^2}\langle I_0 \circ \exp(w)^{-1} - I_1, \\ &\quad \nabla(I_0 \circ \exp(w)^{-1}) \cdot \partial_h \exp(w)^{-1}\rangle_{L^2}\end{aligned} \tag{19}$$

$$\begin{aligned}\partial_h E_3(w) &= \frac{2}{\sigma^2}\langle I_1 \circ \exp(w) - I_0, \\ &\quad \nabla(I_1 \circ \exp(w)) \cdot \partial_h \exp(w)\rangle_{L^2}\end{aligned} \tag{20}$$

The Gateaux derivative of the exponential map is obtained using a first order approximation, $\exp(w) = x + w$. The Gateaux derivative of the inverse exponential map is obtained from the fact $\exp(w)^{-1} = \exp(-w)$. Thus, $\partial_h \exp(w) = h$ and $\partial_h \exp(w)^{-1} = -h$ and

$$\begin{aligned}\partial_h E_2(w) &= -\frac{2}{\sigma^2}\langle (LL^\dagger)^{-1}((I_0 \circ \exp(w)^{-1} - I_1) \cdot \\ &\quad \nabla(I_0 \circ \exp(w)^{-1})), h\rangle_V\end{aligned} \tag{21}$$

$$\begin{aligned}\partial_h E_3(w) &= \frac{2}{\sigma^2}\langle (LL^\dagger)^{-1}((I_1 \circ \exp(w) - I_0) \cdot \\ &\quad \nabla(I_1 \circ \exp(w))), h\rangle_V\end{aligned} \tag{22}$$

Collecting the results in Equations 18, 21, and 22, the Euler-Lagrange equation associated to the energy functional is $\nabla_w E(w) = 2w + \partial_h E_2(w) + \partial_h E_3(w)$.

References

[1] V. Arnold. Mathematical methods of classical mechanics. *Springer-Verlag, Berlin, Germany*, 1989.

[2] V. Arsigny, O. Commonwick, X. Pennec, and N. Ayache. Statistics on diffeomorphisms in a Log-Euclidean framework. *MICCAI 2006, Lecture Notes in Computer Science (LNCS), Springer-Verlag, Berlin, Germany*, 4190:924 – 931, 2006.

[3] B. Avants, P. T. Schoenemann, and J. Gee. Lagrangian frame diffeomorphic image registration: Morphometric comparison of human and chimpanzee cortex. *Med. Image. Anal.*, 10(3):397 – 412, 2006.

[4] M. F. Beg, M. I. Miller, A. Trouve, and L. Younes. Computing large deformation metric mappings via geodesic flows of diffeomorphisms. *Int. J. Comput. Vis.*, 61 (2):139–157, 2005.

[5] B. Dodgas, D. W. Sattuck, and R. M. Leahy. Segmentation of skull and scalp in 3D human MRI using mathematical morphology. *Hum. Brain Map.*, 2005.

[6] P. Dupuis, U. Grenander, and M. Miller. Variational problems on flows of diffeomorphisms for image matching. *Quart. Appl. Math.*, pages 587 – 600, 1998.

[7] D. Ebin and J. Marsden. Groups of diffeomorphisms and the motion of an incompressible fluid. *Ann. of Math.*, 92:102 – 103, 1970.

[8] P. T. Fletcher, S. Joshi, C. Lu, and S. M. Pizer. Principal geodesic analysis for the study of nonlinear statistics of shape. *IEEE Trans. Med. Imaging*, 23(8):994 – 1005, 2004.

[9] L. Garcin and L. Younes. Geodesic matching with free extremities. *J. Math. Imaging Vis.*, 25:329 – 340, 2006.

[10] J. Grabowski. Free subgroups of diffeomorphism groups. *Fundam. Math.*, 131:103 – 121, 1988.

[11] U. Grenander and M. Miller. Computational Anatomy: an emerging discipline. *Quart. Appl. Math.*, 56:617 – 694, 1998.

[12] D. D. Holm, J. T. Ratnanather, A. Trouve, and L. Younes. Soliton dynamics in computational anatomy. *Neuroimage*, 23:170 – 178, 2004.

[13] S. Joshi, B. Davis, M. Jomier, and G. Gerig. Unbiased diffeomorphic atlas construction for compuational anatomy. *Neuroimage*, 23:151 – 160, 2004.

[14] P. Lorenzen, M. Prastawa, B. Davis, G. Gerig, E. Bullitt, and S. Joshi. Multi-modal image set registration and atlas formation. *Med. Image. Anal.*, 10:440 – 451, 2006.

[15] M. I. Miller. Computational anatomy: shape, growth, and atrophy comparison via diffeomorphisms. *Neuroimage*, 23:19–33, 2004.

[16] M. I. Miller, A. Trouve, and L. Younes. Geodesic shooting for computational anatomy. *J. Math. Imaging Vis.*, 24:209–228, 2006.

[17] X. Pennec. Intrinsic statistics on Riemmanian manifolds: Basic tools for geometric measurements. *J. Math. Imag. Vis.*, 25(1):127 – 154, 2006.

[18] R. Schmid. Infinite dimensional lie groups with applications to mathematical physics. *J. Geom. Symm. Phys.*, 1:1 – 67, 2004.

[19] A. Staniforth and J. Cote. Semi-lagrangian integration schemes for atmospheric models-a review. *Monthly Weather Review*, 119:2206 – 2223, 1991.

[20] L. Wang, F. Beg, T. Ratnanather, C. Ceritoglu, L. Younes, J. C. Morris, J. G. Csernansky, and M. I. Miller. Large deformation diffeomorphism and momentum based hippocampal shape discrimination in dementia of the Alzheimer type. *IEEE Trans. Med. Imaging*, 26(4):462 – 470, 2007.

[21] L. Younes. Jacobi fields in groups of diffeomorphisms and applications. *Quart. Appl. Math.*, 65:113 – 134, 2007.